Magnetic Resonance in Medicine 44:884–892 (2000)

Diffusion Tensor MRI of the Spinal Cord

Mario Ries,[1] Richard A. Jones,[1] Vincent Dousset,[2] and Chrit T.W. Moonen[1*]

Apparent diffusion tensor (ADT) measurements on the spinal cord using a pulsed-field-gradient (PFG) multi-shot echo-planar imaging (EPI) sequence are presented. In a study of 10 healthy volunteers, the obtained rotationally invariant anisotropy information is compared to the results obtained by the rotationally dependent methods. The water diffusivity in the direction parallel to the fibers was found to be almost 2.5 times higher than the average diffusivity in directions perpendicular to the fibers and showed cylindrically symmetric anisotropy characteristics. The influence of partial volume effects and the point spread function on the measured results was evaluated, and it was the concluded that a resolution of 1 mm in the read and phase directions is required to obtain unbiased values. Possible clinical implications were demonstrated by investigating the diffusion characteristics of 10 patients suffering from narrowing of the cervical canal. The changes in the diffusion characteristics were found to be large enough to allow a robust detection of diffusion changes in the spine, even in cases in which conventional T_2 and T_1 weighted images were unable to detect any lesion. Magn Reson Med 44: 884–892, 2000. © 2000 Wiley-Liss, Inc.

Key words: diffusion; magnetic resonance imaging; spinal cord; EPI

Diffusion-weighted (DW) imaging has become a well established method for detecting acute ischemia in the brain (1). The possibility of probing neuronal microstructures by diffusion experiments in highly ordered neuronal systems, such as the spinal cord, is an intriguing possibility; however, clinical studies in these regions have been hampered by the presence of susceptibility artifacts arising from the surrounding bony structures, motion due to cerebrospinal fluid (CSF), carotid and vertebral artery pulsations, and respiratory motion. Additional problems arise from the fact that the diffusion measurements on the comparatively small spinal cord can easily be contaminated with signal components arising from the surrounding CSF. This puts additional demands on the in-plane resolution and constrains the use of fast-imaging methods such as single shot DW-EPI or DW-TSE. The first aim of this study was to develop an imaging protocol that facilitates the measurement of the apparent diffusion constant (ADC) and the apparent diffusion tensor (ADT) in the spinal cord in a clinically realistic time-frame. The influence of CSF signal contamination on the precision of the diffusion measurements was evaluated by an analysis of the point spread function (PSF) of the experiment and the partial volume effect. Since the ordered structure of the fibers in the spinal cord may permit assumptions regarding the diffusion symmetries, the diffusion characteristics were measured and analyzed using rotationally dependent and rotationally invariant methods on 10 healthy volunteers. Furthermore, as pathological changes (e.g., those leading to demyelination) within the spinal cord can be expected to induce significant changes in the diffusion anisotropy of the spinal cord, this study also includes an initial evaluation of possible clinical applications by examining 10 patients with narrowing of the cervical canal due to cervical spondylosis. This is a common disease in middle-aged and elderly patients, which is caused by chronic segmental compression of the spinal cord, and can result in a partial demyelination of the fiber structure.

MATERIALS AND METHODS

MRI

All diffusion imaging was performed on a 1.5T clinical MRI system (Philips Medical Systems Best, The Netherlands) equipped with actively shielded magnetic field gradients with a maximal amplitude of 23 mT/m. RF-excitation was performed by the integrated body-coil. A four-element phased-array surface coil with a linear arrangement of the elements was employed for RF-reception. As a control group, 10 healthy volunteers were scanned. The imaging protocol consisted of a T_2-weighted coronal scout scan to localize the exact position of the spinal cord, followed by six diffusion-weighted experiments.

For the diffusion imaging a diffusion-weighted, multi-shot EPI technique was used. *k*-Space was split into 13 equal sections (13 echoes TE_{EPI} = 36 msec) in the second dimension, each of which was encoded by one of the 13 gradient echoes, in linear order. The image matrix was 256 × 195 and the FOV was 230 mm, leading to a nominal voxel size of 0.90 mm × 1.17 mm. Three slices 5 mm thick were acquired per experiment. Diffusion sensitization was obtained by applying two symmetric diffusion gradient pulses before and after the 180° pulse of a preparation SE experiment with an echo time TE_{diff} = 80 msec, resulting in a complete echo time of the sequence of TE = 116 msec. The diffusion sensitizing gradients were applied along six different directions, indicated by vector (x, y, z): $\{(0, 0, 1), (0, 1, 0), (1, 0, 0), (0, 1/\sqrt{2}, 1/\sqrt{2}), (1/\sqrt{2}, 0, 1/\sqrt{2}), (1/\sqrt{2}, 1/\sqrt{2}, 0)\}$ using the following convention: x (phase encode, superior-inferior), y (readout, anterior-posterior), z (slice select, left-right), as suggested by Pierpaoli et al. (2). For the volunteer studies, six *b*-values (0, 120, 240, 360, 480, and 600 s/mm^2) in each direction were obtained; for the patient studies, three *b*-values (0, 300, and 600 s/mm^2) were measured. To minimize bulk motion effects on the diffusion experiments, a navigator echo (3) was acquired and the sequence was triggered from every third R-wave by a pulse oximeter. The

[1]Résonance Magnetique des Systemes Biologiques, UMR 5536, CNRS/Université Bordeaux2, Bordeaux, France.

[2]Service de Neuroradiologie, Hospital Pellegrin, Bordeaux, France.

Grant sponsor: Biomed; Grant number: BMH4-CT98-5058; Grant sponsors: Boehringer Ingelheim Foundation; Conseil Regional d'Aquitaine.

*Correspondence to: Chrit Moonen, UMR 5536/CNRS, Dept. de Résonance Magnetique des Systémes Biologiques, 146 Rue Leo-Saignat, 33076 Bordeaux, France. E-mail: Chrit.Moonen@rmsb.u-bordeaux2.fr

Received 4 January 2000; revised 5 July 2000; accepted 6 July 2000.

complete duration of the diffusion experiment was 31 min for the volunteer studies and 13 min for the patient studies, based on an average heart rate of 60 beats/min. Before Fourier reconstruction, the phase of each readout was corrected according to the navigator data and a Riesz-filter was applied to avoid ringing. Finally, a sagittal T_2-weighted TSE image and a T_1-weighted TSE were acquired for anatomical comparison, and a transversal T_2-weighted image was acquired to ascertain if the lateral position of the spine had changed during the diffusion protocol.

Image Analysis

The diffusion-weighted images were analyzed off-line on a LINUX-workstation using in-house software written in interactive data language (IDL) and C++. The ADC values for all six directions were calculated by applying a Levenberg-Marquard fitting algorithm to a mono-exponential model on a pixel by pixel basis. The ADC values were obtained in regions of interest (ROIs) containing about 100 pixels, which were placed in the center of the spinal cord to avoid contamination by the surrounding CSF.

Whereas in isotropic media one scalar parameter, the ADC, is sufficient to describe the 3D displacement of particles due to diffusion, six independent parameters forming the diffusion tensor are required for anisotropic media. Since the diffusion tensor is always symmetric, it is possible, even in anisotropic media, to find a frame of reference, the principal frame, in which all translational movements appear to be uncorrelated. This diagonalization of the diffusion tensor results in three eigenvalues, each representing the magnitude of the diffusion in the principal directions and the corresponding three eigenvectors, representing the orientations of the three principal directions in the magnet coordinate system (4). While the diagonal elements of the ADT are directly accessible by ADC measurements with a diffusion weighting along the principal magnet directions, the off-diagonal elements of the tensor were obtained by subtracting the oblique ADC-maps according to the principle suggested by Basser et al. (5). The obtained tensor map was finally diagonalized using the Householder reductions and the QL method with implicit shifts (6). For the following discussion, we assume that the eigenvalues of the tensor (λ_1, λ_2, λ_3) are sorted by their magnitude, with λ_1 = highest and λ_3 = lowest magnitude, respectively. Several rotationally invariant parameters representing the tensor characteristics have been proposed (1,2,7). In our analysis, we initially focused on the eigenvalues by evaluating the ratios of the principal diffusivities (7), the volume ratio (8) and the fractional anisotropy (9).

While these ratios provide stable results when used on averaged datasets, their use on a pixel by pixel basis is limited by the signal-to-noise ratio (SNR) of the data: Any attempt to map the ratio of two highly error-biased numbers will result in an image with large signal fluctuations ("salt and pepper noise"); hence, an additional method was employed to visualize the characteristics of all three eigenvectors in one image in which the diffusion values are scaled between 0 and 256, and 256 is assigned to the highest overall diffusion value. The eigenvalues are sorted in descending order, and then one color component of a 24-bit RGB image is assigned according to the following convention: λ_1 is blue, λ_2 is red, and λ_3 is green, as shown in the inset of Fig. 6. This leads to the following visualization results: extremely anisotropic structures appear in a color range from black to clear blue, depending on their magnitude. Isotropic regions, such as within the CSF, result in colors ranging over the full gray-scale.

The structural anatomy of the spinal cord was investigated by mapping the main fiber direction (2,10–14). This information was obtained from the eigenvectors corresponding to λ_1 on a pixel by pixel basis. From a variety of suggested color schemes for directionally-encoded color (DEC) maps (15–17) the color scheme suggested by Jones et al. (15) was chosen to visualize the main fiber direction in a 2D image, as shown in the inset of Fig. 8.

Influence of the PSF and Partial Volume Effects

The PSF determines the smallest resolvable structure within an imaging experiment and the amount of signal contamination between neighboring voxels (18). The PSF of an EPI experiment is, apart from the FOV and the employed phase encoding, mainly influenced by the signal decay during the acquisition train. This signal decay is determined by T_2^* and, to a lesser extent, by T_2 (19,20). In addition to the inherent variations in the PSF of the different tissues, local susceptibility variations introduce additional local variations in T_2^*, resulting in a highly spatially dependent PSF. Therefore, a spatially resolved measurement of the PSF in vivo, as suggested by Robson et al. (21), was implemented. This method employs an additional phase-encoding gradient before the conventional echo-planar acquisition which can be placed in the read, phase, and slice directions depending on the desired direction of the PSF measurement, resulting in a 4D dataset. It can be shown that the Fourier reconstruction of this fourth encoding direction results in a spatially resolved map of the PSF multiplied with the integral over the spin density within the FOV (21). To evaluate the influence of the measured PSFs on the results of the diffusion measurements, a computer simulation was performed. A simple model was created by assigning the signal amplitudes and an estimate of the diffusion values of CSF and spinal-cord tissue to two neighboring signal sources of 1.5 cm diameter, as shown in Fig. 1. The diffusion tensor of the CSF was assumed to be isotropic ($\lambda_1 = \lambda_2 = \lambda_3 = 3.0 \cdot 10^{-9}$ m^2/s), and the diffusion tensor of the spinal cord tissue was assumed to be cylindrically symmetric ($\lambda_1 = 2.0 \cdot 10^{-9}$ m^2/s, $\lambda_2 = \lambda_3 = 1.0 \cdot 10^{-9}$ m^2/s). The diffusion experiment was simulated by convoluting these signal sources separately with their measured PSFs. By weighting these two datasets with their assigned diffusion tensor, and adding the complex data for the two signals for each *b*-value, a synthetic dataset of a full DW-EPI experiment was created. Finally, a complete diffusion analysis of this simulated, compound object was performed and analyzed.

To evaluate the influence of partial volume effects in the slice direction, a transverse image of the spinal cord was segmented within an area reflecting the slice thickness of a sagittal DW-EPI experiment, as shown in Fig. 2. The segmented CSF and spinal cord tissue were then weighted with the appropriate signal amplitudes obtained from the

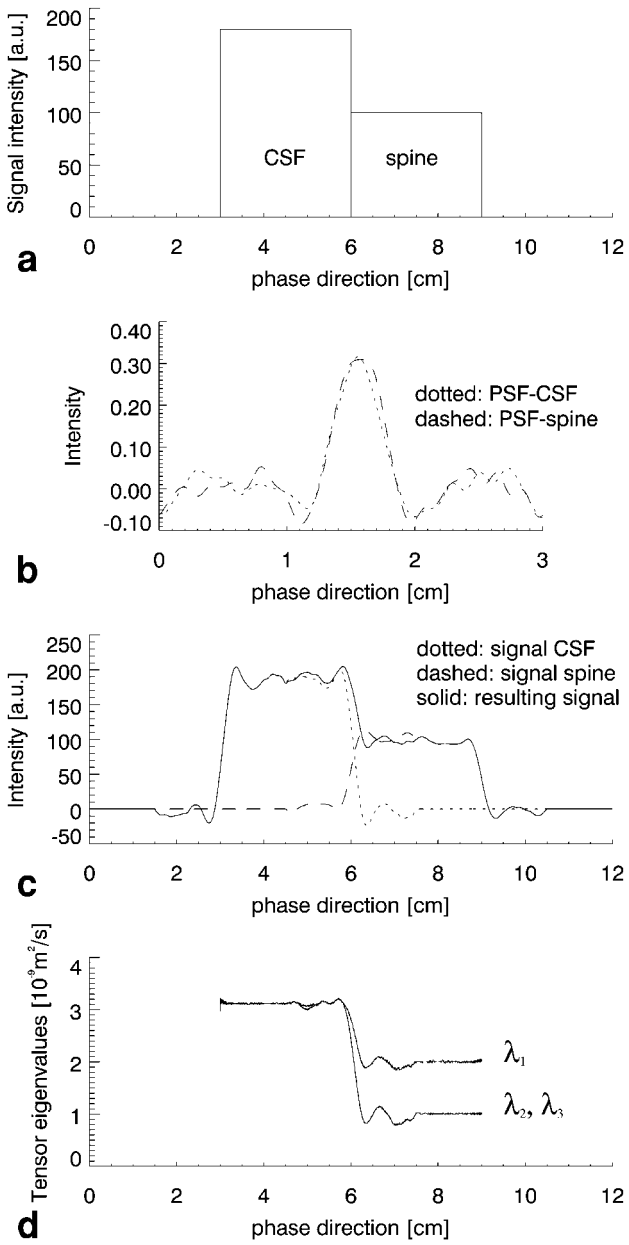

FIG. 1. **a:** Simple model of two neighboring signal sources for the evaluation of the influence of signal contamination on diffusion measurements. **b:** The measured PSFs of spinal cord tissue and the CSF. **c:** The resulting image obtained by convoluting the measured PSFs with the simulated signal sources. **d:** The propagation of the CSF signal into spinal cord regions introduces severe errors in the obtained eigenvalues.

DW-EPI images. Finally, the signals were projected in the phase direction on the read-axis of the transversal scan. The result, as shown in Fig. 2, represents the signal behavior in the read direction of a sagittal image of the spinal cord, but contains additional information regarding from which tissue the signal components originate. By assigning the same diffusion characteristics as described above, a synthetic dataset of a full diffusion experiment can be constructed and analyzed.

RESULTS

Control of the Experimental Setup

The ADCs and the eigenvalues of the ADT for free water, ethanol, and dimethylsulphoxide were measured and found to be in good accordance with the literature values (23). The influence of the cross-terms, as evaluated by comparing the off-diagonal elements of the tensor within a water phantom to the results obtained from a region in the noise, showed that all contributions were within the noise level. Furthermore, the analysis of the ADCs acquired with opposite gradient polarity (22) showed no significant contributions of the cross-terms to the diffusion attenuation over the whole evaluated range.

Figure 1b shows the PSF in the phase direction of the multi-shot DW-EPI taken in the center of the spinal cord in

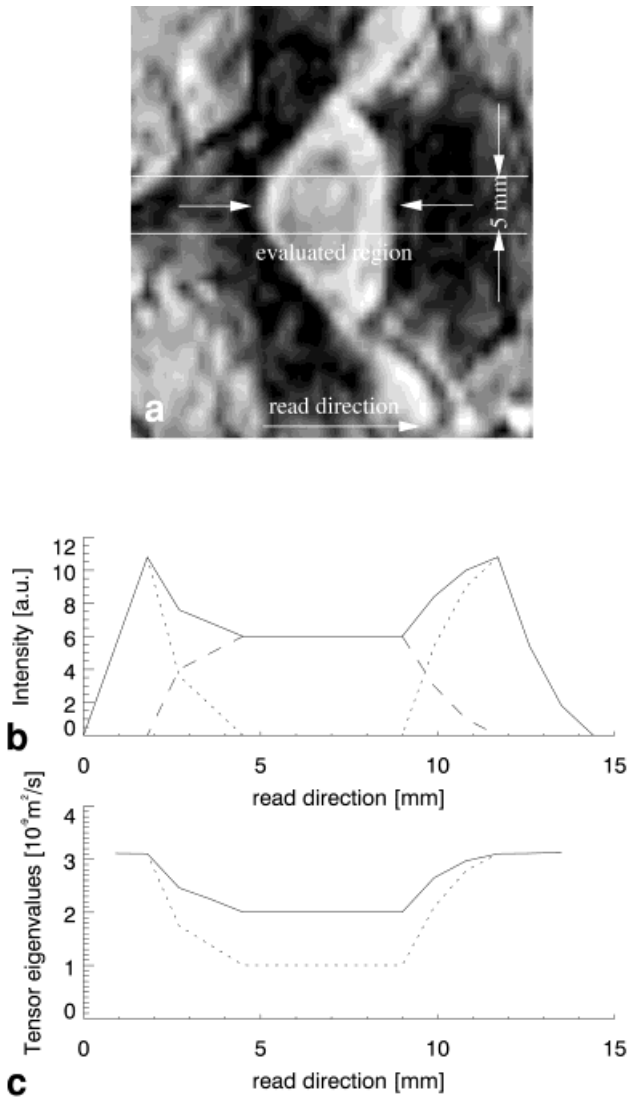

FIG. 2. **a:** A transversal image used to separate the signal components occurring within a slice of a sagittal DW-EPI. **b:** Signal contributions along the read-direction: the dotted curve shows the signal contribution due to the CSF, the dashed line due to the spinal cord tissue, and the solid line the resulting signal. **c:** The calculated eigenvalues of the simulated system (λ_1: solid, λ_2: dashed).

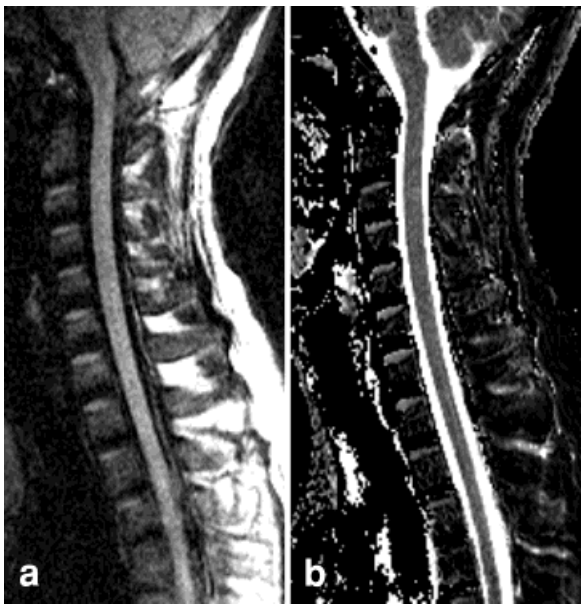

FIG. 3. **a:** Diffusion-weighted image with b = 360 s/mm^2. **b:** ADC-trace map of a healthy volunteer.

comparison with the PSF measured in the surrounding CSF. The full-width half-maximum (FWHM) of 1.27 mm reflects a loss of 9% resolution compared to the nominal resolution of 1.17 mm. The 1.50 mm FWHM of the PSF within the spinal cord results in a loss of 28% resolution. Figure 1d shows the eigenvalues of a simulated system representing neighboring regions of CSF and spinal cord tissue, as shown in Fig. 1a, that were derived by taking the PSF into account.

Figure 2a shows a typical axial TSE image that was used to segment the indicated area in order to evaluate the signal contributions from spinal cord tissue and CSF due to partial volume effects. These data were used to simulate the signal contributions within a slice of sagittal DW-EPI of 5-mm slice thickness, as shown in Fig. 2b. Since the correct diffusion characteristics can be assigned to the signal contributions, a diffusion analysis results in the eigenvalues as displayed in Fig. 2c. Accurate values for the eigenvalues and anisotropy indices are obtained only from the central 50% of the spine. Since slight lateral movements can further degrade the results by moving the slice out of the spine, a post-diffusion control of the position using an axial image has to be performed.

ADC Spinal Cord

Figure 3 shows a typical DW image and the ADC-trace image obtained from a healthy volunteer. The mean ADC values in the anterior-posterior, superior-inferior, and left-right directions in the spinal cord are given in Table 1. All values were taken in regions where the spinal cord was parallel to the superior/inferior-axis of the measurement frame. As a first assumption, the myelin-fibers can be expected in this region to be parallel/orthogonal to the diffusion weighting. Since the geometry of the spinal cord intuitively suggests cylindrical symmetry of the diffusion anisotropy (24) a *t*-test (25) was applied to the diffusion values in the anterior-posterior and left-right directions. The measured data supports this hypothesis within a confidence-level of $\alpha = 0.10$. The post-diffusion position control showed that two of the volunteers moved slightly during the examination, shifting the spinal cord partially out of the evaluated slice. The data from these two examinations were excluded from the study.

Figure 4 shows T_2- and diffusion-weighted images from a patient suffering from cervical canal narrowing due to cervical spondylosis. Figure 5 shows the ADC maps from the same patient. The measured ADC and eigenvalues for all 10 patients studied are presented in Table 2. Two sets of ADC values are presented: one taken in ROIs directly in the affected region, the other set in normal tissue in ROIs 5–10 cm above or below, depending on the exact location of the lesion where neither the T_2 nor the diffusion images showed any abnormalities. In all patients, the obtained ADC images showed a significant change of the diffusion characteristics in the region of the lesion. In four cases the ADC_{SI} is more than one SD higher than the diffusion constant of water at 37°C, and thus cannot be explained purely by diffusion effects. The diffusion-weighted image in Fig. 4 shows clearly that these high values can not be completely accounted for by the influence of contaminating CSF signal due to partial volume effects. The CSF signal is at a *b*-value of $b = 300$ s/mm^2, already decreased below the detection limit, while the spinal cord tissue with its lower ADC remains visible above and below the

Table 1
The ADC-Measurements, the Eigenvalues of the ADT and the Fractional Anisotropy (FA) of the Spinal Cord [$\cdot 10^{-9}$ m^2/s)] of Eight Healthy Volunteers

Subject	ADC_{SI}	ADC_{AP}	ADC_{LR}	$\frac{2ADC_{SI}}{ADC_{AP} + ADC_{LR}}$	λ_1	λ_2	λ_3	FA
1	2.33 ± 0.45	0.68 ± 0.26	0.97 ± 0.29	2.83 ± 0.78	2.48	1.19	0.11	0.75
2	2.25 ± 0.40	1.04 ± 0.38	0.67 ± 0.26	2.64 ± 0.79	3.06	1.15	−0.93	1.02
3	2.00 ± 0.44	1.17 ± 0.33	0.65 ± 0.31	2.19 ± 0.64	2.92	1.12	−0.008	0.82
4	1.83 ± 0.62	0.79 ± 0.45	0.51 ± 0.38	2.81 ± 1.43	2.45	1.46	−0.034	0.76
5	2.35 ± 0.89	1.02 ± 0.41	0.72 ± 0.42	2.70 ± 1.16	3.68	1.67	−0.93	0.97
6	2.30 ± 0.91	1.03 ± 0.40	0.95 ± 0.52	2.33 ± 1.02	3.05	1.34	−0.21	0.85
7	2.26 ± 0.82	0.87 ± 0.42	0.86 ± 0.43	2.61 ± 1.22	2.91	1.12	−0.13	0.85
8	2.05 ± 0.54	0.73 ± 0.30	0.90 ± 0.49	2.53 ± 0.95	3.45	1.35	0.76	0.65
average ± σ	2.17 ± 0.18	0.92 ± 0.16	0.77 ± 0.15	2.58 ± 0.21	3.00 ± 0.39	1.30 ± 0.18	−0.17 ± 0.52	0.83 ± 0.11

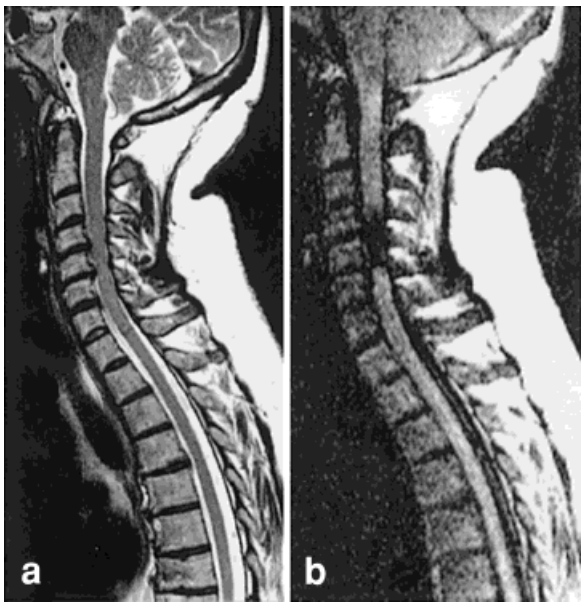

FIG. 4. Although the compression of the cervical canal is clearly visible on the T_2-weighted image (**a**), no internal damage of the spinal cord can be seen. The diffusion-weighted image (b = 300 s/mm^2 in LR-direction) (**b**) shows a clear signal drop in the compressed region.

lesion. The signal decrease (81%) of the spinal cord in the compressed area at this *b*-value cannot be explained by CSF artifacts because of the low CSF volume fraction.

ADT Spinal Cord

Tables 1 and 2 give the eigenvalues, the volume ratio, and the fractional anisotropy of the calculated ADT evaluated in the same regions as used for the ADC data. The error calculation performed in Ref. 2 for highly anisotropic systems with cylindrical symmetry shows that the tensor eigenvalues obtained from data with an SNR between 10 and 20 result in a typical systematic fitting error: For a simulated system with: $\lambda_1 = 1.5 \cdot 10^{-9}$, $\lambda_2 = 0.2 \cdot 10^{-9}$, $\lambda_3 = 0.2 \cdot 10^{-9}$ [m^2/s] this error causes the calculated eigenvalues λ_1 to be underestimated by 0–10%, λ_2 to be overestimated by 5–25% and λ_3 to be underestimated by 15–100%. This explains the calculated negative eigenvalues λ_3 that are physically impossible. Figures 6 and 7 show the color representation of the eigenvalues of the ADT of a healthy volunteer and a patient, respectively, and Figs. 8 and 9 show the corresponding main fiber direction maps in the DEC representation.

DISCUSSION

General Considerations

Although the diffusion cross-term behavior of the DW-EPI sequence on phantoms was shown to be negligible using two independent experimental setups, it has to be taken into account that cross-terms arising from susceptibility variations within the spinal cord might introduce an unknown error bias into the in vivo experiments. The analysis of the influence of the PSF (as shown in Fig. 1) shows that tensor measurements of the spinal cord in the vicinity of tissue transitions can lead to errors of 25% (an error analysis of the ADC measurements leads to the same conclusion). This error propagates into the calculation of ratio of the principal diffusities, the volume ratio and the fractional anisotropy. Taking the nominal resolution of 1.17 mm in the phase direction into account, this means that the results of all voxels in the direct vicinity of CSF/cord transitions have to be discarded in order to obtain unbiased values. However, an even more severe error is introduced by the partial volume effect in the slice direction. The spinal cord shown in Fig. 2 has a diameter of

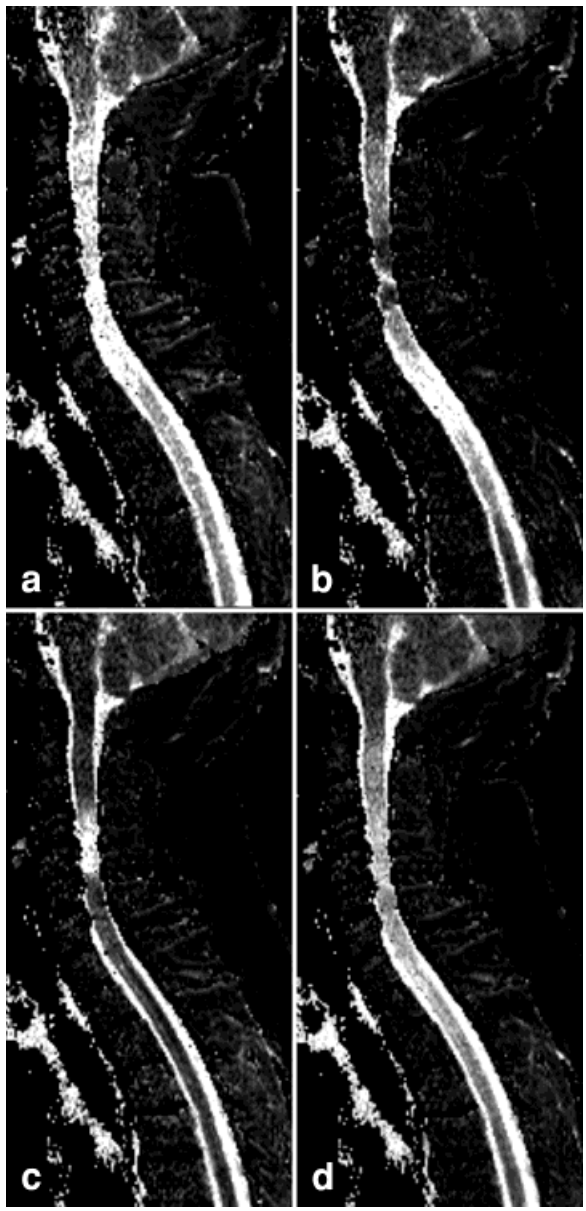

FIG. 5. ADC maps of the patient shown in Fig. 4. **a:** The ADC_{SI} (phase direction) is elevated over a region that exceeds the acute lesion. Since the compression affects the spinal cord in the anterior-posterior direction, the mechanical deformation of the fibers results in different changes in the ADC_{AP} and the ADC_{LR}, as shown in **b** and **c**. **d:** Trace.

Table 2
Comparison of the ADCs [$\cdot 10^{-9}$ m^2/s], the Eigenvalues of the ADT and the Fractional Anisotropy (FA) of Ten Patients With Cervical Canal Narrowing Due to Cervical Spondylosis*

Subject	ADC_{SI}	ADC_{AP}	ADC_{LR}	λ_1	λ_2	λ_3	FA
1. Unaffected	4.05 ± 0.56	1.47 ± 0.49	1.43 ± 0.49	5.23	1.67	−0.25	0.87
1. Injured	5.36 ± 0.84	1.77 ± 0.91	1.83 ± 0.52	7.08	2.09	−0.32	0.88
2. Unaffected	1.68 ± 0.54	1.07 ± 0.41	0.51 ± 0.42	1.98	1.01	−0.06	0.79
2. Injured	4.98 ± 1.06	3.56 ± 1.88	3.30 ± 1.05	7.32	3.71	0.53	0.72
3. Unaffected	2.40 ± 0.89	1.18 ± 0.52	1.06 ± 0.55	2.70	0.96	0.12	0.79
3. Injured	5.18 ± 1.12	1.32 ± 0.80	3.99 ± 1.06	6.56	3.69	0.06	0.75
4. Unaffected	1.86 ± 0.39	0.56 ± 0.25	0.63 ± 0.32	2.13	0.79	0.18	0.76
4. Injured	3.64 ± 1.07	1.49 ± 0.29	1.02 ± 0.21	4.21	1.42	0.42	0.76
5. Unaffected	2.16 ± 0.68	1.27 ± 0.32	0.93 ± 0.41	2.75	0.74	−0.12	0.89
5. Injured	2.65 ± 1.05	1.06 ± 0.45	0.67 ± 0.49	3.35	1.22	−0.09	0.84
6. Unaffected	2.35 ± 1.09	1.47 ± 0.70	0.80 ± 0.48	3.25	1.18	0.10	0.80
6. Injured	5.17 ± 1.17	1.05 ± 0.57	1.63 ± 0.74	5.77	1.41	−0.42	0.92
7. Unaffected	2.56 ± 1.36	1.02 ± 0.58	0.55 ± 0.31	4.16	1.83	0.06	0.78
7. Injured	2.36 ± 1.09	4.51 ± 1.65	2.67 ± 1.57	6.80	3.49	0.03	0.77
8. Unaffected	1.99 ± 0.65	1.26 ± 0.45	1.01 ± 0.73	3.06	1.28	0.18	0.76
8. Injured	2.72 ± 0.85	1.79 ± 0.69	1.42 ± 0.31	2.99	1.76	0.32	0.66
9. Unaffected	2.45 ± 1.13	1.40 ± 0.81	1.09 ± 0.42	3.01	1.26	0.30	0.73
9. Injured	3.95 ± 1.33	0.95 ± 0.55	0.81 ± 0.43	4.61	0.96	−0.03	0.9
10. Unaffected	2.45 ± 0.48	1.34 ± 0.38	1.44 ± 0.32	2.94	1.76	0.46	0.62
10. Injured	3.21 ± 0.51	2.19 ± 0.35	1.41 ± 0.30	5.05	2.11	−0.72	0.91

*The first values are taken in an unaffected region, the second in the injured area, respectively.

10 mm measured in the anterior-posterior direction; however, only a region of about 7 mm can be identified on a sagittal image as genuine spinal cord tissue, due to partial volume artifacts from the adjoining CSF (Fig. 2a). From this remaining area, only the diffusion values obtained in a region of 5 mm diameter are not severely biased by signal contributions from the CSF (Fig. 2b). Close to the boundaries of a selected region, the error for the eigenvalues increases up to 25% for λ_1, and over 75% for λ_2 and λ_3. Considering the nominal resolution of 1.17 mm in the phase direction and 0.9 mm in the read direction, all values obtained from areas less than two pixels away from the visible spinal cord boundary have to be considered as heavily error biased. This can be seen by a comparison of the images in Fig. 3. Due to the high *b*-value in the diffusion-weighted image the CSF-signal is almost completely suppressed, while on the calculated ADC-trace image its signal influence dominates the results of the boundary zone. As a result, the spinal cord appears to be smaller on the ADC-trace image. This behavior restricts the choice of the ROI for ADC and ADT evaluations to small regions in the center of the visible spinal cord. Furthermore, the resolution and the contrast of the experiment is not sufficient to distinguish between white and gray matter within the cord. Non-pathologic fluctuations in the substructure of the cord might lead to ADC/ADT modifications that appear as a pathology. Nevertheless, none of these modifications were found among the control studies or outside the injured regions of the patients. Finally, the diffusion measurements are very sensitive to subconscious movements, such as swallowing, that result in a slight change in the position of the head and the upper spinal cord during the imaging session. To ascertain if such changes have occurred, a verification of the lateral position of the spinal cord at the end of the imaging session is required.

Volunteer Studies

Taking these restrictions into account, the data from the healthy volunteers presented in Table 1 shows that the presented method leads to reproducible ADC measurements that are in good agreement with previously published results (26).

Furthermore, the results show that the diffusion in the spinal cord is clearly anisotropic, with the ratio of the mean ADC values $2ADC_{SI}/ADC_{AP} + ADC_{LR}$ for all volunteers being close to 2.6. A possible explanation for this anisotropy might be the model of hindered diffusion suggested by Le Bihan et al. (27) that predicts (for white matter) a ratio of the mean ADC values of ≈ 2.47.

Since healthy spinal cord is a highly ordered neuronal fiber bundle, structural damage might be easily detected by characterizing the isotropy of the diffusion within the fiber bundle. As with diffusion studies on brain tissue, there are basically two ways of obtaining this information: by deriving rotationally variant anisotropy indices from the ADC data, or by measuring the complete diffusion tensor and calculating the anisotropy indices from the eigenvalues of the tensor.

The justification of the first method relies on the assumption that the tissue can be always orientated in the magnet such that the applied diffusion gradients are precisely along the principal directions of the cord. However, while this is generally possible in the slice direction (left-right direction) in the anterior-posterior and superior-inferior directions, these assumptions hold for only a relatively small section due to the curvature of the spine. The deviations of the spinal cord from the gradient directions in our study were typically between 0 and 25°. If the diffusion values obtained in regions where the spine is well aligned with the diffusion gradients are compared

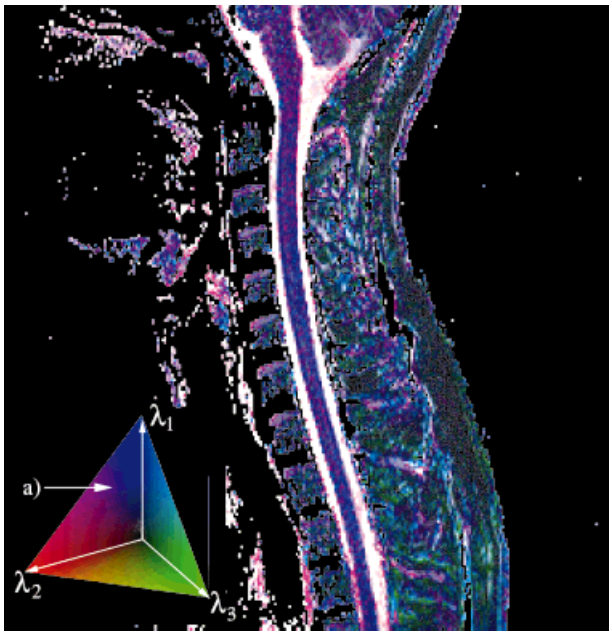

FIG. 6. Eigenvalues of the ADT of the healthy volunteer shown in Fig. 3 in a color representation. Color legend: The highest color values at the end of each axis represents in this graph a diffusion value of $\lambda_n = 3.1 \cdot 10^{-9}$ m^2/s. Since the eigenvalues get sorted by magnitude ($\lambda_1 \geq \lambda_2 \geq \lambda_3$), anisotropic diffusion results in colors located near the λ_1-axis. The anisotropic diffusion of moderate magnitude ($\lambda_1 = 2.5$, $\lambda_2 = 1.2 \cdot 10^{-9}$ m^2/s) in the spinal cord results therefore in a violet color. Isotropic diffusion of high magnitude, such as in the CSF, is represented by white. The marked point **a** represents the diffusion anisotropy resulting from the eigenvalues $\lambda_1 = 2.4 \cdot 10^{-9}$ m^2/s, $\lambda_2 = 1.1 \cdot 10^{-9}$ m^2/s, and $\lambda_3 = 0$ m^2/s.

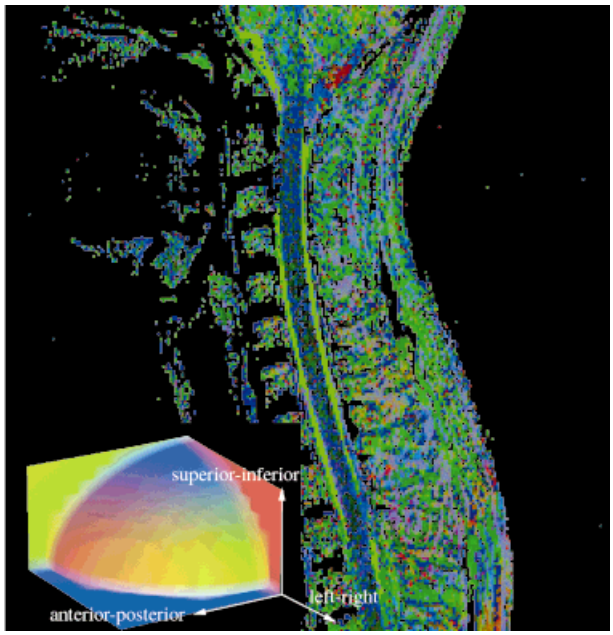

FIG. 8. Fiber direction map of a healthy volunteer. The blue color of the spinal cord represents a fiber orientation in the superior-inferior direction, as shown in the color legend. At the brain stem the orientation of the fibers diverges, and the colors change to a mixture of green, red, and blue.

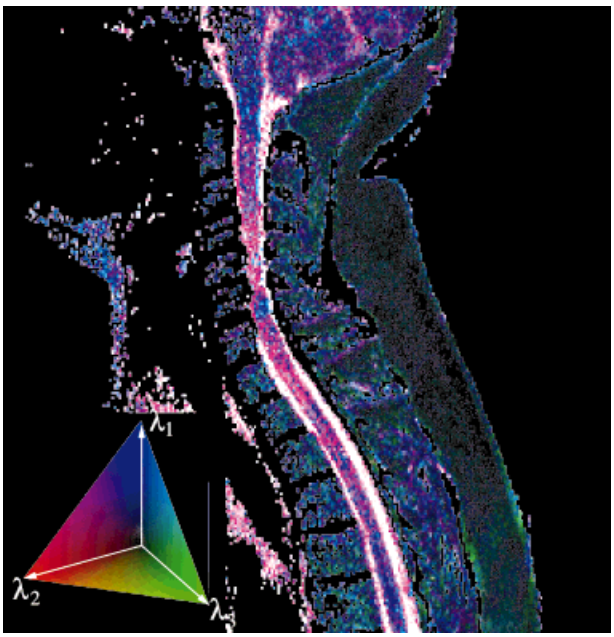

FIG. 7. Eigenvalues of the ADT of the same patient as shown in Fig. 5. The dark violet color of the unaffected bottom part of the spinal cord represents normal diffusion anisotropy and magnitude. The light blue regions higher up show that the magnitude of the diffusion is elevated.

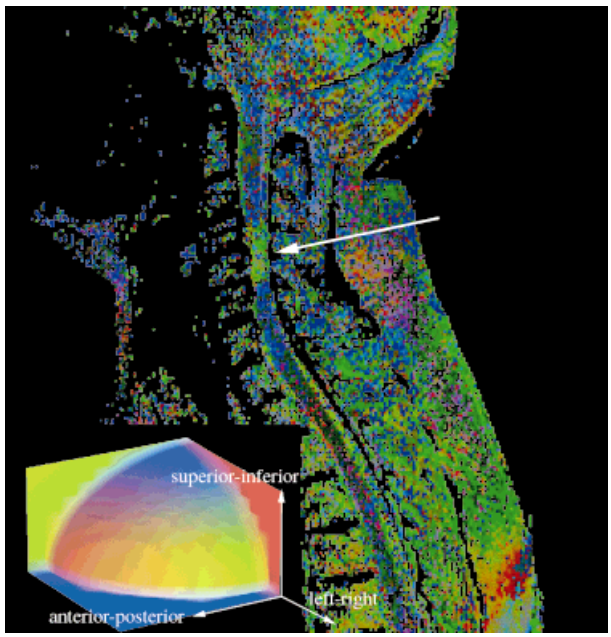

FIG. 9. Fiber direction map of a patient suffering cervical canal narrowing. The blue color above and below the marked region of the canal narrowing reflects a normal fiber orientation in the superior-inferior direction. The distinct green zone within the lesion shows a change in this direction toward the left-right direction caused by fiber damage.

with those from regions where the principal directions of the spinal cord deviate from the direction of the diffusion gradients by an angle α, the apparent ADC_{SI} and the ADC_{SI} are biased by:

$$ADC_{SI_{app}} = ADC_{SI}\cos^2(\alpha) \cdot ADC_{AP}\sin^2(\alpha)$$

$$ADC_{AP_{app}} = ADC_{AP}\cos^2(\alpha) \cdot ADC_{SI}\sin^2(\alpha).$$

While this error might be negligible for regions of small deviations, the values representing the anisotropy information, such as in the ratio of the principal diffusivities $ADC_{SI_{app}}/ADC_{AP_{app}} + ADC_{LR_{app}}$ are biased by an error of 16.4% for $\alpha = 25°$.

Although this error bias can be completely removed by the use of rotationally invariant anisotropy information obtained from the eigenvalues of the diffusion tensor, the results are still biased by the noise of the experiment. Since the typical SNR of our studies was 12–16, we have to take the extensive error analysis by Basser et al. (2) into account when interpreting the data. Due to the systematic underestimate of λ_3 the ratios of all anisotropy indices that have λ_3 in the denominator show large fluctuations.

This made it almost impossible to interpret the ratio of the principal diffusivities and meant that the volume ratio images that were acquired with an SNR less than 15 were of little value. The fractional anisotropy provides much more stable results in the presence of occasional negative values of λ_3, but still reflects a full quantitative measure of the "magnitude" of the anisotropy of the ADT.

Patient Studies

Since the aim of this study was not to characterize cervical spondylosis, but to show the potential clinical relevance of diffusion measurements, we do not discuss the various results of the patient data in detail but focus on the common characteristics. The major advantage of diffusion imaging is that while T_2- and T_1-weighted images clearly showed the narrowing of the cervical canal they were, in all 10 cases, not sensitive to pathological changes within the spinal cord itself.

In comparison, the ADC images showed in all 10 cases a significant change in the diffusion characteristics within spinal cord lesions, in good agreement with the results obtained by Castillo et al. (29) using a diffusion-weighted SSFP sequence. The ADC values increased, on average, in the inferior/superior direction by around 100%, in the anterior/posterior direction by 50%, and in the left/right direction by 50%. These strong variations allowed, in general, a good identification of the affected region. A single cause of these large diffusion changes cannot be identified at this stage. Since the link between spinal cord compression and myelopathy has been established (28), part of these findings can be explained by an increased permeability of the membranes due to chronic hypoperfusion and a subsequent partial destruction of the membranes. Another possible contributing factor suggested by Castillo et al. (29) is that the chronic compression of the spinal cord leads to an abnormal motion of the CSF in the subarachnoid space and might force CSF into the cord itself, leading to the formation of intramedullary microcysts. The resulting transmedullary movement of the CSF might be due to a pressure-related transport mechanism across membranes or via dilated perivascular spaces, which could account for the extreme high diffusion values with anisotropic diffusion characteristics observed in 50% of the examined cases.

Figure 5 shows some of the typical diffusion characteristics that were found in the patient studies: The ADC_{SI} shows higher values in an area that is far larger than the area of compression depicted on the T_2 images. The ADC_{AP} and ADC_{LR} values were only abnormal in a well-defined area which corresponded more closely to the area of compression. Furthermore, it is remarkable that while the ADC_{LR} is elevated in the upper part of the visible canal narrowing, the ADC_{AP} is elevated in an area below it.

This is the first hint that the diffusion properties in the healthy spinal cord might reflect cylindrical symmetry, but that this may not be true in damaged regions. The full extent of the affected area could, in most cases, only be estimated by comparing the results of all three directions.

The analysis of the tensor information provides further insights into this behavior, and Figure 7 shows the eigenvalues in color. Compared to the results obtained from a healthy volunteer (shown in Fig. 6), the diffusion characteristics of the lower part of the spinal cord are found to be normal. Higher up, an increasing diffusion in the direction of the main ADT axis (reflected by the increase of the brightness of the blue color in the image) can be observed. The purple region within the canal narrowing marks a zone in which the character of the diffusion changes more towards isotropic diffusion. By taking the directional information obtained from the eigenvectors into account, as displayed in Fig. 9, further insights into the character of the lesion can be gained: The blue color above and below the region of the canal narrowing reflects the normal behavior, namely that the direction of the main semi-major axis of the diffusion tensor is parallel to the spinal cord. But the distinct green zone within the lesion shows a change of this direction towards the slice (left-right) direction. A possible explanation for this surprising result might be severe myelin fiber canal deformation due to the mechanical compression. This nonsymmetric diffusion behavior explains the distinctly elevated ADC_{AP} and ADC_{LR} regions in Fig. 5.

Although a full analysis of the pathological changes is beyond the scope of this paper, it is evident that demyelination does not fully explain our results. Additional abnormal CSF flow and transmedullary movement, as suggested by Castillo et al. (29) is compatible with our observations.

CONCLUSIONS

Despite the low SNR of the diffusion measurements and the influence of partial volume effects, the changes in the diffusion characteristics caused by pathological changes of the tissue seem to be large enough to allow a robust detection of diffusion changes in the spine. This allows diffusion imaging techniques to localize structural fiber damage in the spinal cord, even in cases where conventional T_2 and T_1 weighted images were unable to detect any lesion.

In most cases the measurement of ADC values in two or three directions is sufficient to estimate the extent and exact location of the damage. Nevertheless, the full assessment of the diffusion tensor provides a better understanding of the underlying changes in the physiology and may permit a more accurate diagnosis. The question of whether anisotropy information can differentiate between reversible and irreversible fiber damage is closely linked to the question of which factors contribute to these modifications, and needs to be addressed by further clinical studies.

ACKNOWLEDGMENTS

The authors thank Pr. Pointillard for his support on patient issues, Dr. Jason Brookes for sharing the task of developing the off-line reconstruction for the PSF experiments, and Dr. Erik Dumont for valuable suggestions. This work was supported by a Ph.D. fellowship from the Boehringer Ingelheim Foundation for M. Ries, and a Biomed grant (BMHR-CT98-5058) from the European Union for R.A. Jones.

REFERENCES

1. van Gelderen P, Vleeschouwer MHM, DesPres D, Pekar J, van Zijl PCM, Moonen CTW. Water diffusion in acute stroke. Magn Reson Med 1994; 31:154–163.
2. Pierpaoli C, Basser PJ. Toward a quantitative assessment of diffusion anisotropy. Magn Reson Med 1996;36:893–906.
3. Ordidge RJ, Helpern JA, Qing Z, Knight RA. Correction of motional artifacts in MR diffusion-weighted images. In: Proceedings of SMRM, 11th Annual Meeting, Berlin, 1992. p 1209.
4. Basser PJ. Inferring microstructural features and the physiological state of tissues from diffusion weighted images. NMR in Biomedicine 1995; 8:333–343.
5. Pierpaoli C, Basser PJ. A simplified method to measure the diffusion tensor from seven MR images. Magn Reson Med 1998;39:928–934.
6. Press WH, Vetterling WT, Teukolsky SA, Flannery BP. Numerical recipes in C. Cambridge: Cambridge University Press; 1996. p 470–478.
7. Basser PJ, Matinello J, Le Bihan D. MR diffusion tensor spectroscopy and imaging. Biophys J 1994;66:259–267.
8. Pierpaoli C, Mattinello J, Le Bihan D, Di Chiro G, Basser PJ. Diffusion tensor imaging of brain white matter anisotropy. In: Proceedings of SMR, 2nd Annual Meeting, San Francisco, 1994. p 1038.
9. Basser PJ, Pierpaoli C. Microstructural and physiological features of tissues elucidated by quantitative-diffusion-tensor MRI. J Magn Reson Series B 1996;111:209–219.
10. Ulug A, Bakht O, Bryan R, van Zijl P. Mapping of human brain fibers using diffusion tensor imaging. In: Proceedings of the 4th Annual Meeting of ISMRM, New York, 1996. p 1325.
11. Conturo TE, McKinstry RC, Akbudak E, Robinson BH. Encoding of anisotropic diffusion with tetraedal gradients: a general mathematical diffusion formalism and experimental results. Magn Reson Med 1996; 35:399–412.
12. Tang CY, Lu D, Wei TC, Spiegel J, Atlas S, Buchenbaum MS. Image processing techniques for the eigenvectors of the diffusion tensor. In: Proceedings of the 5th Annual Meeting of ISMRM, Vancouver, Canada, 1997. p 2054.
13. Davis T, Van Wedeen J, Weisskoff R, Rosen B. White matter tract visualisation by echo-planar MRI. In: Proceedings of the 4th Annual Meeting of ISMRM, New York, 1996. p 289.
14. Basser PJ, Mattiello J, LeBihan D. MR imaging of fiber tract direction and diffusion in anisotropic tissues. In: Proceedings of the 4th Annual Meeting of ISMRM, New York, 1996. p 288.
15. Jones D, Williams S, Horsfield M. Full representation of white matter fiber direction on one map via diffusion tensor analysis. In: Proceedings of the 5th Annual Meeting of ISMRM, Vancouver, Canada, 1997. p 1743.
16. Pierpaoli C. Oh no! One more method for colour mapping of fiber tract direction using diffusion MRI imaging data. In: Proceedings of the 5th Annual Meeting of ISMRM, Vancouver, Canada, 1997. p 1741.
17. Pajevic S, Pierpaoli C. Color schemes to represent the orientation of anisotropic tissues from diffusion tensor data: application to white matter fiber tract mapping in the human brain. Magn Reson Med 1999;3:526–540.
18. Rossman K. Point spread-function, line spread-function, and modulation transfer function: tools for the study of imaging systems. Radiology 1969;93:257–272.
19. Farzaneh F, Riederer SJ, Pelc NJ. Analysis of T_2 limitations and off-resonance effects on spatial resolution and artifacts in echo-planar imaging. Magn Reson Med 1990;14:123–139.
20. Constable RT, Gore JC. The loss of small objects in variable TE imaging: implications for FSE, RARE and EPI. Magn Reson Med 1992;28:9–24.
21. Robson MD, Gore JC, Constable RT. Measurement of the point spread function in MRI using constant time imaging. Magn Reson Med 1997; 38:733–740.
22. Neeman M, Freyer JP, Sillerud LO. A simple method for obtaining cross-term-free images for diffusion anisotropy studies in NMR microimaging. Magn Reson Med 1991;21:138–143.
23. Holz M, Weingartner H, Sacco A. In: Bruker Almanac, Bruker analytische Messtechnik GmbH, Karlsruhe; 1996. p 128.
24. Gulani V, Iwamoto GA, Jiang H, Shimony JS, Webb AG, Lauterbur PC. A multiple echo pulse sequence for diffusion tensor imaging and its application in excised rat spinal cords. Magn Reson Med 1997;38:868–873.
25. Bronstein IN, Semendjajev KA. Handbuch der Mathematik. Moskau: Teubner Verlag, Stuttgart und Nauka Verlag; 1991. p 22,687–688.
26. Clark CA, Barker GJ, Tofts PS. Magnetic resonance diffusion imaging of the human cervical spinal cord. Magn Reson Med 1999;41:1269–1273.
27. Le Bihan D, Turner R, Douek P. Is water diffusion restricted in human brain white matter? An echo-planar NMR imaging study. Neuro Report 1993;4:887–890.
28. Nagata K, Kiyonaga K, Ohasi T, Sagara M, Myazaki S, Inoue A. Clinical value of magnetic resonance imaging for cervical myelopathy. Spine 1990;15:1088–1096.
29. Castillo M, Arbelaez A, Fisher LL, Smith JK, Mukherji SK. Diffusion-weighted imaging in patients with cervical spondylosis. Int J Neuroradiol 1999;5:79–85.